Intermetallic disordered magnet $Gd_2Pt_{1.1}Ge_{2.9}$ and its relation to other AlB_2-type compounds

L. S. Litzbarski,[1,2,3,*] M. J. Winiarski,[1,2] T. Klimczuk,[1,2] M. Łapiński,[1,2] M. Pugaczowa-Michalska,[4] P. Skokowski,[4] and B. Andrzejewski[4]

[1]*Faculty of Applied Physics and Mathematics, Gdansk University of Technology, Narutowicza 11/12, 80-233 Gdansk, Poland*
[2]*Advanced Materials Center, Gdansk University of Technology, Narutowicza 11/12, 80-233 Gdansk, Poland*
[3]*Department of Mechatronics and High Voltage Engineering, Faculty of Electrical and Control Engineering, Gdansk University of Technology, Narutowicza 11/12, 80-233 Gdansk, Poland*
[4]*Institute of Molecular Physics, Polish Academy of Science, Smoluchowskiego 17, 60-179 Poznan, Poland*

(Received 29 October 2021; accepted 7 February 2022; published 24 February 2022)

The intermetallic germanide $Gd_2Pt_{1.1}Ge_{2.9}$ was synthesized using an arc-melting method. The crystal structure was characterized using powder x-ray diffraction, revealing a disordered ternary AlB_2-type structure (space group $P6/mmm$, No. 191) with lattice parameters $a = 4.2092(1)$ Å and $c = 4.0546(2)$ Å. Physical properties were investigated by magnetic susceptibility and heat capacity measurements, which indicated onset of antiferromagnetic order at $T_t = 8$ K. The obtained properties were compared with the ones reported for other members of the AlB_2-type Gd_2TGe_3 (T = Ni, Cu, and Pd) family. The magnetic ordering in these compounds was discussed in terms of their crystal structure and the influence of Gd ions.

DOI: 10.1103/PhysRevB.105.054427

I. INTRODUCTION

Ternary RE_2TX_3 intermetallic compounds (RE = rare earth, T = transition metal, X = semimetal) are prospective materials rich in phenomena and potential technical applications, for example, Er_2NiSi_3, which is a promising candidate for a magnetic refrigerant material [1]. These features can be regarded because of interaction between RE ions and layered crystal structure. This is mostly related to the fact that RE_2TX_3 compounds often belong to aristotype AlB_2 ($P6/mmm$, No. 191 [2], see Fig. 1), which is one of the simplest crystal structures. This structure may be represented by triangular Al layers (Wyckoff position $1a$) alternating along the c axis with layers of B ($2d$). The B atoms form honeycomb graphitelike layers, where the distance between neighboring atoms is $d = \frac{a}{\sqrt{3}} \approx 1.7$ Å for AlB_2. In general, many structural variants of intermetallics can be derived from the AlB_2 aristotype by replacing Al and B atoms and/or distorting the lattice. The relationship between various AlB_2-derived structures was thoroughly discussed by Hoffman and Pöttgen [3].

The best known AlB_2-type compound is MgB_2, which was reported as a superconductor with a high $T_c = 39$ K [4]. This discovery aroused significant excitement and prompted many researchers to undertake efforts to synthesize compounds with the AlB_2-like structure.

The honeycomb layers of the ternary RE_2TX_3 with AlB_2-type structure are occupied by T and X atoms and separated by layers of RE ions. This structure can exist in two variants that differ in c/a ratio, i.e., ordered and disordered. In the ordered variant, the a parameter value is about two times larger than c ($c/a \approx 0.5$) like, for example, in U_2IrSi_3 [5] or Ca_2PdGe_3 [6]. The second variant is a disordered structure with lattice parameter $c/a \approx 1$ where T and X atoms are randomly distributed over the honeycomb lattice. The statistical distribution of T and X ions in graphitelike layers causes a variation of local environment around RE ions, which promote the magnetic cluster formation. Moreover, in this type of structure, the strengths of interactions between nearest neighbors (NN) and next-NNs (NNNs) are comparable, which is one of the essential sources of magnetic frustration [7]. For these reasons, a lot of reported RE_2TX_3 compounds exhibit spin-glass-like behavior, e.g., Er_2NiSi_3 [1], Tb_2PdSi_3 [8], and Nd_2PtGe_3 [9]. Furthermore, there are also reported extraordinary physical phenomena for members of the RE_2TX_3 family such as a Kondo effect observed in Ce_2NiGe_3 [10] and a double magnetic transition in Pr_2NiGe_3 at 12 and 5.5 K [10]. Another example of intriguing properties is superconductivity, observed in disordered 2:1:3-type compounds with nonmagnetic RE ions, e.g., Y_2PtGe_3 ($T_c = 3.3$ K) [11], Y_2PdGe_3 ($T_c = 3.0$ K) [12], and La_2NiGe_3 ($T_c \approx 0.45$ K) [10]. Pakhira *et al.* [13] proposed that vacancies are essential to get chemically pure RE_2TX_3 compounds, as it was applied to synthetize, i.e., $Tm_2Ni_{0.93}Si_{2.93}$. We propose an alternative method which is based on changing the $T : X$ ratio deliberately to obtain $RE_2T_{1+x}X_{3-x}$ composition. This method was already successfully applied to synthesize chemically pure ternary intermetallics $Tb_2Pd_{1.25}Ge_{2.75}$, $Dy_2Pd_{1.25}Ge_{2.75}$ [14], and $Ho_2Pd_{1.3}Ge_{2.7}$ [15].

In this paper, we report on successful synthesis of an intermetallic compound $Gd_2Pt_{1.1}Ge_{2.9}$ and compare its properties with other known members of the Gd_2TGe_3 family: Gd_2CuGe_3 [16], Gd_2NiGe_3 [10], and Gd_2PdGe_3 [17]. The experimental investigation includes magnetic properties and specific heat analysis.

*leszek.litzbarski@pg.edu.pl

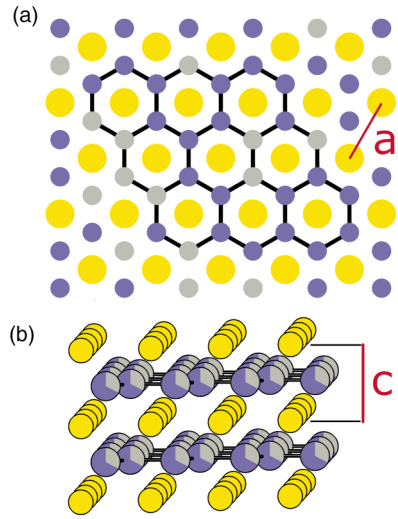

FIG. 1. Crystal structure of $Gd_2Pt_{1.1}Ge_{2.9}$ with a disordered ternary AlB_2 structure variant. Big spheres are Gd; small represent Pt and Ge. Panel (b) was generated using VESTA software [18].

II. EXPERIMENTAL

Polycrystalline samples of $Gd_2Pt_{1+x}Ge_{3-x}$ ($x = 0$–0.3) were synthetized from appropriate amounts of high-purity constituent elements, i.e., Gd (99.9%, Onyxmet), Pt (99.5%, Alfa Aesar), and Ge (99.999%, Alfa Aesar). The expected loss of Gd was compensated by adding an extra amount of this element (∼2% molar excess). Obtained mixtures were melted in an inert atmosphere (Zr-gettered high-purity argon gas) inside an arc furnace (MAM-1 Edmund Buhler GmbH). The ingot was turned over and remelted several times to ensure homogeneity. The overall change in weight after the synthesis process was negligible (∼0.5%), which indicates that the actual alloying level was close to the assumed elemental concentration. The final products were crushed and checked by powder x-ray diffraction (pXRD) carried out on a Bruker D2Phaser diffractometer equipped with a XE-T detector (Cu K_α radiation). The FULLPROF package was used for Rietveld analysis of the pXRD data. Samples of Gd_2TGe_3 compounds (T = Ni, Pd, or Cu) were synthesized using the same method, as it is described in the Supplemental Material [19].

The valence states of the elements were analyzed by x-ray photoemission spectroscopy (XPS) to confirm that magnetic properties of compounds are not affected by the presence of Gd- and transition metal-containing oxide impurities. Before the measurements, the surface of samples was etched for 15 min by an Ar ion gun (FDG 150 ion source mounted in the analytic chamber). The XPS measurement was carried out using Omicron NanoScience ultrahigh vacuum equipment. Samples were measured at room temperature at pressures $<1.1 \times 10^{-8}$ mBar. The photoelectrons were excited by a Mg-K_α x-ray source operated at 15 keV and 300 W. An Argus hemispherical spectrophotometer equipped with a 128-channel detector was used for photoelectron energy measurements. The data analysis was performed with the CASA XPS software, using a Shirley background subtraction and a Gauss-Lorentz curve fitting algorithm by the least-squares method—GL(30). Results of XPS measurements are presented in the Supplemental Material [19].

The magnetic properties of $Gd_2Pt_{1+x}Ge_{3-x}$ samples were examined through a series of experiments performed with a Quantum Design Physical Property Measurement System with a vibrating sample magnetometer. The magnetization measurements were recorded for different applied magnetic field values (up to 9 T) both in a zero-field-cooling (ZFC) mode as well as in a field-cooling (FC) mode. The specific heat measurements were collected with and without an applied magnetic field using a standard thermal relaxation technique in the temperature range 1.9–300 K.

The density functional calculations were done within the projector augmented wave method [20,21] as implemented in the Vienna *Ab initio* Simulation Package [22,23]. For the calculations based on the generalized gradient approximation (GGA), we used the exchange-correlation functional according to the Perdew-Burke-Ernzerhof (PBE) formulation [24]. In many cases, a GGA as well as a local density approximation (LDA) or a local spin density approximation (LSDA) has well-known limitation when applied to the systems with a strong electron correlation. For rare earth elements (lanthanides), the more the valence electrons in atoms are localized, the more their atomic properties are conserved in the solid state. Thus, one of the essential features of rare earth compounds is the fact that the f shell is spatially located around the nucleus. Both the pure band approach and the artificial treatment of the $4f$ electrons as a core state for Gd metal [25,26] did not bring satisfactory compatibility with experimental data. The difficulty in describing both band behavior and localized behavior has led to the concept of the Hubbard model combined with first principles LDA (or LSDA) in a computational scheme called LDA + U [27]. Thus, more advanced electronic structure methods (LSDA + U [27]) have resulted in the proper ground state of Gd [25] and the $4f$ splitting close to the experimental data [28,29]. In our density functional theory (DFT) calculations of Gd_2PtGe_3, we refer to the widely used approach based on the correlated band structure. The f states were included in valence for the Gd atom. Moreover, the Hubbard U correction (PBE + U) in the rotationally invariant form of Dudarev *et al.* [30] has also been applied to treat the localized Gd-$4f$ electronic states. Various studies of Gd and Gd-related systems often provide a similar value of Hubbard corrections in DFT + U calculations [31–34]. However, as noted in Ref. [28], the value of the Hubbard interaction U is much more difficult to estimate because the constrained LSDA calculation does not necessarily provide the ultimate value to be used in a LDA + U or GGA + U study. Moreover, the optimal U parameter provided in Ref. [28] allowed the GGA + U and LDA + U methods to correctly describe both the experimental XPS and Bremsstrahlung Isochromat Spectroscopy (BIS). It should be noted that the value of the parameter U is different from that in the previously mentioned papers [31–34]. To put things into a wider perspective, in the presented calculation, the magnitude of U is varied between 0 and 10 eV for the Gd-$4f$. To achieve a balanced description of Gd_2PtGe_3 with the $P6/mmm$ structure with an experimental observation, the dependence of selected observables on the effective U parameter has been investigated. We also assumed the ferromagnetic (FM)

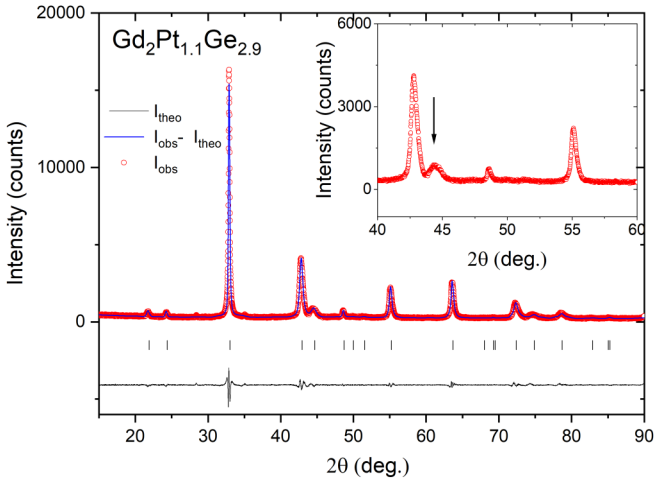

FIG. 2. Le Bail refinement of powder x-ray diffraction (XRD) data for $Gd_2Pt_{1.1}Ge_{2.9}$. Experimental data and calculated intensity are represented by red circles and blue lines, respectively. The difference is shown in the lower part by solid black lines. Black vertical ticks correspond to Bragg peaks for the space group $P6/mmm$ (No. 191). The inset shows the enlarged plot for $40^\circ < 2\theta < 60^\circ$ range. The (002) reflection at $\sim 45^\circ$ marked by an arrow is strongly broadened compared with neighboring (110), (111), and (201) at 43°, 48°, and 50°.

and antiferromagnetic (AFM) orders and the relaxation of cells.

A kinetic energy cutoff of 520 eV and a total energy convergence threshold of 10^{-6} eV were used. The force convergence criterion of 10^{-7} eV/Å during the structural relaxation was adopted. The first Brillouin zone was sampled by using a Γ-centered 16 × 16 × 14 k-point grid.

III. RESULTS AND DISCUSSION

Analysis of pXRD patterns indicates that fully stoichiometric Gd_2PtGe_3 reveals the presence of a small amount of a parasitic phase, which can be indexed as $GdPt_2Ge_2$ (tetragonal $ThCr_2Si_2$-type structure). This impurity phase cannot be removed by thermal annealing of the ingot. The pure samples can be synthesized by deliberately changing occupation of honeycomb sites by Pt and Ge. In this way, the single-phase sample is achieved with the nominal stoichiometry $Gd_2Pt_{1.1}Ge_{2.9}$. The refinement is presented in Fig. 2. For simplicity, we will refer to this compound as Gd_2PtGe_3. The crystal structure of the Gd_2PtGe_3 was verified to be AlB_2 type, and crystallographic data are provided in Table I. We have also observed an anisotropic broadening effect—the $00l$ reflections are much more broadened than the others. Such a phenomenon was previously reported for other members of the RE_2TGe_3 family, e.g., $Tb_2Pd_{1.25}Ge_{2.75}$ [14] and Nd_2PtGe_3 [9]. To account for the broadening, we used the quartic model of anisotropic strain implemented in the FULLPROF program [35] to improve fitting of the lattice parameters to the pXRD patterns.

For Gd_2TGe_3, the lattice parameters scale with the size of the transition metal atom, which is easy to observe as a contraction of the c parameter and expansion of the a parameter (Table II). However, in contrast to what was observed for the Nd_2TGe_3 system [9], the volume of the unit cell does not increase monotonously with the increase of radius of T atoms. The smallest value of volume of the unit cell was found for the Gd_2CuGe_3. This phenomenon may be explained by the comparable ionic radius of Cu and Ge, which leads to the closest packing of honeycomb layers. Comparing the lattice parameters of the Gd_2TGe_3 compounds, we can conclude that the c/a ratio ≈ 1. This minor difference between c and a lattice parameters is responsible for comparable values of the NN and the NNN exchange interaction strength [1]. Lack of superstructure reflections (which were observed in Ca_2PdGe_3 and Ca_2PtGe_3 [6]) suggests the presence of occupational disorder within the T-Ge plane. The coexistence of site disorder and magnetic frustration provides conditions for formation of glassy magnetic order [36] and causes many of the RE_2TX_3 compounds, e.g., $Tm_2Ni_{0.93}Si_{2.93}$ [13], Er_2NiSi_3 [1], and $Ho_2Ni_{0.95}Si_{2.95}$ [10], to show spin-glass-like properties. To investigate the nature of magnetic ordering in the intermetallic compound Gd_2PtGe_3, we performed physical properties measurements.

TABLE I. Refined structural parameters for an intermetallic compound $Gd_2Pt_{1.1}Ge_{2.9}$.

Cell formula	$Gd(Pt_{0.55}Ge_{1.45})$
Space group	$P6/mmm$ (No.191)
a (Å)	4.2092 (1)
c (Å)	4.0546(2)
V (Å^3)	62.212(4)
Molar weight (g mol^{-3})	739.7
Density (g cm^3)	5.94
RE ($1a$)	$x = y = z = 0$
Pt ($2d$)	$x = \frac{1}{3}; y = \frac{2}{3}; z = 0.5$
Ge ($2d$)	$x = \frac{1}{3}; y = \frac{2}{3}; z = 0.5$
Figures of merit	
R_p (%)	14.4
R_{wp} (%)	14.2
R_{expt} (%)	8.31
χ^2	2.93

The XPS analysis excluded the contamination of studied samples with impurities, which could impact the magnetic measurement results. No characteristic peaks for oxides were detected on high-resolution spectra.

The temperature dependence of DC magnetic susceptibility χ is plotted in Fig. 3. The $\chi(T)$ curve was obtained for an applied magnetic field value of 0.01 T. At high temperatures, Gd_2PtGe_3 exhibits paramagnetic behavior, which can be observed as an increase of $\chi(T)$ with decreasing temperature. This phenomenon may be described by the Curie-Weiss law expressed by the following equation:

$$\chi = \frac{C}{T - \theta_{CW}},$$

where C is the Curie constant, and θ_{CW} is the Curie-Weiss temperature. A linear fit to the inverse of the DC magnetic susceptibility (inset of Fig. 3) was performed in the temperature

TABLE II. Comparison of the structure parameters and the transition temperature for Gd_2TGe_3 compounds.

	R_{ion} (Å)	R_T/R_{Ge}	a (Å)	c (Å)	V (Å^3)	c/a	T_t (K)
Gd_2NiGe_3 [10]	0.83	0.95	4.053	4.101	59.03	1.012	10
Gd_2CuGe_3 [16]	0.87	1.00	4.079	4.089	58.85	1.002	12
Gd_2PtGe_3	0.94	1.08	4.20917	4.05463	62.212	0.963	8
Gd_2PdGe_3 [17]	1.00	1.15	4.2146	4.049	62.286	0.961	10

range 10–300 K. The fit of the Curie-Weiss law to the experimental data resulted in a value of $\theta_{CW} = -12.8(3)$ K, which indicates AFM interactions between magnetic moments.

The obtained value of C was used to calculate an effective magnetic moment, which is given by the expression:

$$\mu_{\text{eff}} = \left(\frac{3Ck_B}{\mu_B^2 N_A}\right)^{1/2},$$

where k_B is the Boltzmann constant, μ_B is the Bohr magneton, and N_A is the Avogadro number. The value of $\mu_{\text{eff}} = 7.45(1)\,\mu_B$ is only slightly smaller than the theoretical free moment value ($\mu_{\text{theo}} = g_J\sqrt{J(J+1)} = 7.94\,\mu_B$ [37]) expected for the Gd^{3+} ion. The deviation of the calculated moment from its theoretical value is $< 7\%$, which may be explained as an acceptable measurement error. The trivalent nature of the Gd ion was earlier reported for other members of the Gd_2TGe_3 family.

In the main panel of Fig. 3, a peak in the low-temperature region can be observed, which may indicate the onset of AFM ordering. However, a similar upturn is also observed for glassy materials, e.g., RE_2NiSi_3 [10], U_2TSi_3 [38], and $Nd_2Ni_{0.94}Si_{2.94}$ [39]. To clarify which type of order exists in Gd_2PtGe_3, we have measured the AC magnetization as a function of temperature for various frequencies (not shown here). In the case of glassy materials, the maximum in the real part of the AC susceptibility $\chi'(T)$ should shift toward higher temperature with increasing frequencies [36]. This phenomenon was not observed (see Fig. S5 of the Supplemental Material [19]), which may suggest the long-range character of magnetic ordering in Gd_2PtGe_3. On the other hand, this compound exhibits an ageing effect (see Fig. S6 of the Supplemental Material [19]), which is observed for spin-glass-like materials during the remnant magnetization measurements described in detail in our previous works [9,14,15]. However, this feature is sometimes exhibited by materials with long-range magnetic ordering, which was discussed in the literature [40]. It is worth noting that all known Gd_2TGe_3 intermetallic compounds [16,17] are reported as AFMs which exhibit some features of spin-glass-like compounds. It contrasts with their homologues with other lanthanide elements, which are typical cluster glass materials.

The ZFC and FC susceptibility data are plotted in Fig. 4. Both ZFC and FC curves exhibit an upturn at about $T = 10$ K and tend to deviate from each other below this temperature. It should also be observed that the temperature of the bifurcation between ZFC and FC curves is sensitive to the applied magnetic field and shifts to lower temperatures with increasing H. Moreover, this bifurcation exists even at $\mu_0 H = 1$ T, which more evidence for AFM ordering rather than a spin-glass-like transition. Thus, a cusp observed in Fig. 4 may be identified as a point of the paramagnetic-AFM phase transition for Gd_2PtGe_3. The transition temperature T_t was given as a maximum of $d(\chi T)/dT$ for $\mu_0 H = 0.01$ T, and it is equal to $T_N = 8$ K. This value is close to data obtained for other Gd_2TGe_3 compounds (see Table III). Here, T_N is useful to estimate a frustration parameter proposed by Ramirez [7] $f = |\theta_{cw}|/T_T$. The calculated value of $f = 1.6$ suggests

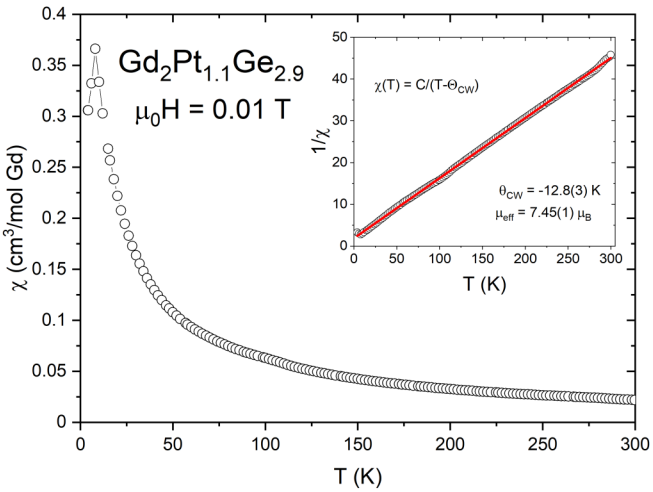

FIG. 3. The temperature dependence of the magnetic susceptibility for $Gd_2Pt_{1.1}Ge_{2.9}$. The inset shows inverse magnetic susceptibility in function of temperature.

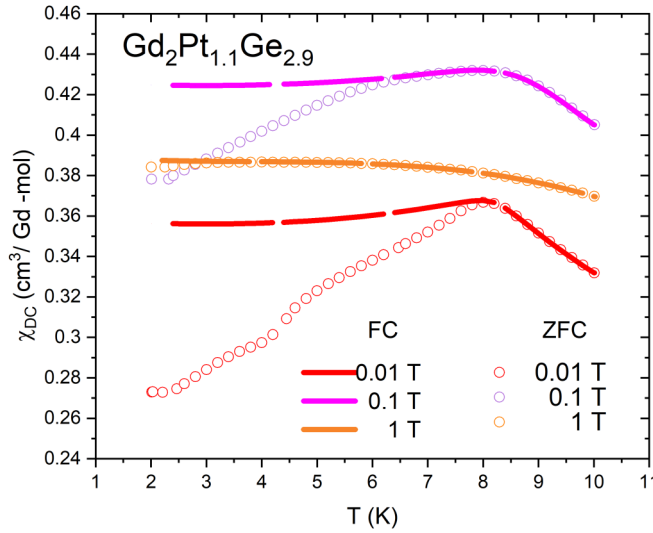

FIG. 4. The zero-field-cooled (ZFC) and field-cooled (FC) curves of magnetic susceptibility for $Gd_2Pt_{1.1}Ge_{2.9}$ compound for different applied magnetic field values.

TABLE III. Selected physical property data for $Gd_2Pt_{1.1}Ge_{2.9}$.

	Gd_2CuGe_3 [16]	Gd_2NiGe_3 [10]	Gd_2PdGe_3 [17]	Gd_2PtGe_3
T_N (K)	12	8	10	8
f	1.5	1.4	0.6	1.6
θ_{CW} (K)	−18	−11.3	−6	−12.8(3)
μ_{eff} (μ_B)	8	8.0	8	7.45(1)
$C_{p,\,peak}$ (J/mol K)	20	–	21	20.5

existence of magnetic frustration, although of comparatively weak strength. Therefore, Gd_2PtGe_3 can be classified as a moderately frustrated magnetic system compound.

Magnetization isotherms measured as a function of the magnetic field for Gd_2PtGe_3 are shown in Fig. 5. The high-temperature curves are linear, which is typical for Curie-Weiss paramagnets. In contrast, $M(H)$ plots obtained at temperatures near T_N exhibit nonlinear dependence on the magnetic field H. Furthermore, these curves do not show any appreciable hysteresis. It should also be observed that the magnetization of this compound does not attain saturation even in high magnetic fields up to $\mu_0 H = 9$ T. Another noteworthy feature is that the value of M for the highest magnetic field is substantially lower than the theoretical value corresponding to Gd^{3+}. These findings are in line with our expectations and confirm that Gd ions exhibit AFM order below $T = 8$ K. Similar behavior was also reported for other members of the Gd_2TGe_3 family.

Heat capacity C_p measurements were carried out to get more information about the magnetic transition in a low-temperature region. In Fig. 6, the results of C_p as a function of temperature measured without an external magnetic field are presented.

Noticeably, the C_p plot attains a saturation value at room temperature, which is consistent with the Dulong-Petit limit: $3nR \approx 150\,\mathrm{J\,mol^{-1}\,K^{-1}}$, where n is the number of atoms

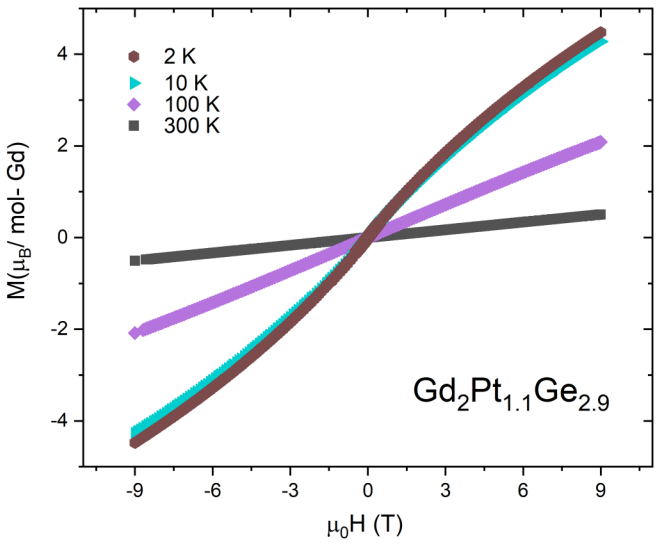

FIG. 5. Isothermal magnetization as a function of an applied magnetic field of Gd_2PtGe_3 for different temperatures.

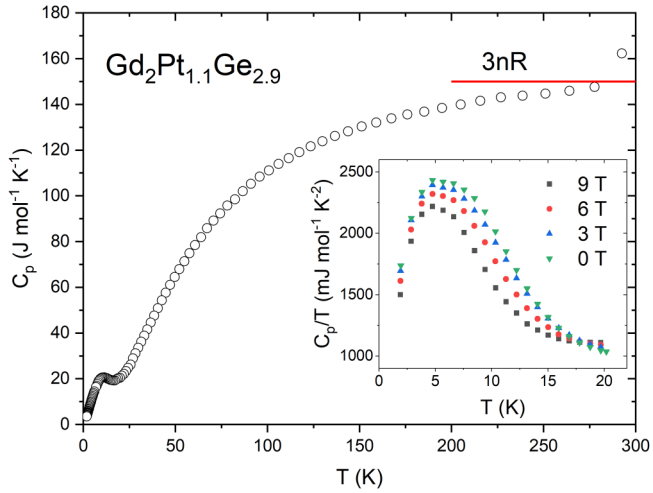

FIG. 6. Temperature dependence of the heat capacity for $Gd_2Pt_{1.1}Ge_{2.9}$. The inset shows plot of C_p/T vs T at low temperatures measured for $\mu_0 H = 0$–9 T.

per formula unit ($n = 6$), and R is the gas constant ($R = 8.314\,\mathrm{J\,mol^{-1}\,K^{-1}}$). At low temperatures, a very visible peak appears in the vicinity of T_N, which confirms the bulk character of the magnetic transition in Gd_2PtGe_3. A maximum value of C_p for this hump exceeds 20 J/mol K, which is expected for equal-moment magnetic structure and is consistent with simple AFM ordering in this compound [41]. The inset of Fig. 6 shows a C_p/T vs T dependence for $\mu_0 H = 0$ and 3 T. The peak around T_N is rather broad and is only weakly affected by the external magnetic field. For AFM materials with a well-ordered crystal structure, a sharp peak is usually expected, while a broad peak is typical for spin-glass materials; however, Gd_2TGe_3 compounds previously described in the literature also exhibit this feature. The broadening of the specific heat anomaly may set from the presence of structural disorder in these materials. Moreover, this phenomenon is usually observed in frustrated AFM systems, which do not exhibit glassy behavior, e.g., $Cu_9Cl_2(cpa)_6$ [42], $PbCuTe_2O_6$ [43], and $KCoPO_4$ [44].

All the reported Gd_2TGe_3 compounds show an AFM behavior but with some features of the spin-glass state (e.g., slow relaxation of ordered moment), while most of the known RE_2TGe_3 materials are found to have a typical spin-glass or cluster-glass transition below their spin-freezing temperature with all the features of a glassy state, including pronounced shift of the transition temperature with increasing excitation frequency. The explanation of this phenomenon seems to be a challenging task, which requires careful insight into the origin of magnetism in RE_2TGe_3 compounds. Physical properties of the abovementioned compounds arise from the coexistence of the layered structure and the strong electron correlation effect of the lanthanide $4f$ electrons, which was described in detail in the literature [2,3].

It was noted in various families of lanthanide-bearing intermetallics that the presence of the orbital component of the total angular momentum (lacking in the case of Gd^{3+}, $J = \frac{7}{2}$, $S = \frac{7}{2}$, $L = 0$) usually increases magnetic frustration [45–47], which can lead in some cases to a formation of a glassy

magnetic state, while the homologous compounds with Gd show long-range order. This underlines the role of single-ion anisotropy in the magnetic frustration and spin/cluster-glass behavior.

To gain insight into the electronic structure of Gd_2PtGe_3, we performed density functional calculations assuming the hypothetical perfect 1:3 Pt : Ge stoichiometry. Pure PBE calculation ($U = 0$ eV) for Gd_2PtGe_3 results in the locations of narrow $4f$ occupied and unoccupied bands of Gd near the Fermi level E_F (at -4.4 and 0.7 eV with respect to E_F, respectively). The $4f$ exchange splitting is almost identical to that obtained in the LDA calculation for the bulk Gd and the Gd surfaces in Refs. [25,26], whereas various photoemission and reverse photoemission studies show that the occupied and unoccupied $4f$ Gd bands shift downward in energy. The neglect of the strong correlation of the $4f$ electrons leads to the incorrect prediction of experimentally observed features in the photoemission spectrum. Previously cited in Ref. [48], DFT studies of bulk Gd and Gd(0001) surface indicate that the neglect of the strong correlation of the $4f$ electrons leads to the wrong prediction of ground state as well as to substantial errors in the magnetic moments and exchange splitting. Petersen *et al.* [48] have demonstrated that a gradient-corrected DFT combined with a Hubbard-like description of the onsite Coulomb repulsions in the $4f$ band (the PBE + U method) leads to an improved description of the physical properties of Gd.

To check how reliable the prediction of PBE + U is with the value of parameter U, for which the ground state of the bulk hexagonal close-packed (hcp) Gd and the Gd surfaces has been successfully predicted in Refs. [31–34,48], we used the value of $U = 6.0$ eV for Gd_2PtGe_3. Unfortunately, the total energy difference between AFM and FM orderings $\Delta E = E_{\uparrow\downarrow} - E_{\uparrow\uparrow}$ (13.4 meV/f.u.) is positive. Thus, the FM ground state of Gd_2PtGe_3 is incorrectly preferred with $U = 6$ eV. Therefore, we considered it worthwhile to perform the calculations for Gd_2PtGe_3 with the U parameter varied from 0 to 10 eV. The PBE and PBE + U functionals favor the AFM coupling between the Gd ions in Gd_2PtGe_3 for $U = 7$ eV and for $0 \leqslant U \leqslant 2$ eV. The total energy of Gd_2PtGe_3 with AFM-ordered Gd ions in a $P6/mmm$ structure is at least 2 meV/f.u. above the FM one for U parameter changes between 2 and 7 eV. The difference between the AFM and FM states in total energy increases in favor of the FM state at the value of the parameter $U = 8$, 9, and 10 eV. For both AFM and FM, the calculated value of the Gd magnetic moment is underestimated (>4%) in comparison with the experimental value of μ_{eff} [dashed line in Fig. 7(a)]. Moreover, the inclusion of the Hubbard U does not affect the theoretical value of the magnetic moment of the Gd ion for $0 \leqslant U \leqslant 8$ eV, as can be seen in Fig. 7(a). However, the increase of the U parameter has the effect of pushing the $4f$ states away from the Fermi level. For $U = 7$ eV, the PBE + U calculation leads to the proper AFM ground state of Gd_2PtGe_3, and the exchange splitting of $4f$ states is enhanced, resulting in a 11.9 eV splitting of occupied and unoccupied $4f$ states of Gd. Results for the density of states (DOS) obtained from such calculations are shown in Figs. 7(b) and 7(c). The electronic structure of Gd_2PtGe_3 in the energy region between -11.8 and -8 eV has a character of Ge s states. The Pt $4d$, Ge $4p$, and Gd $5d$ electronic states are mostly located below the Fermi energy ($E_F = 0$ eV). In

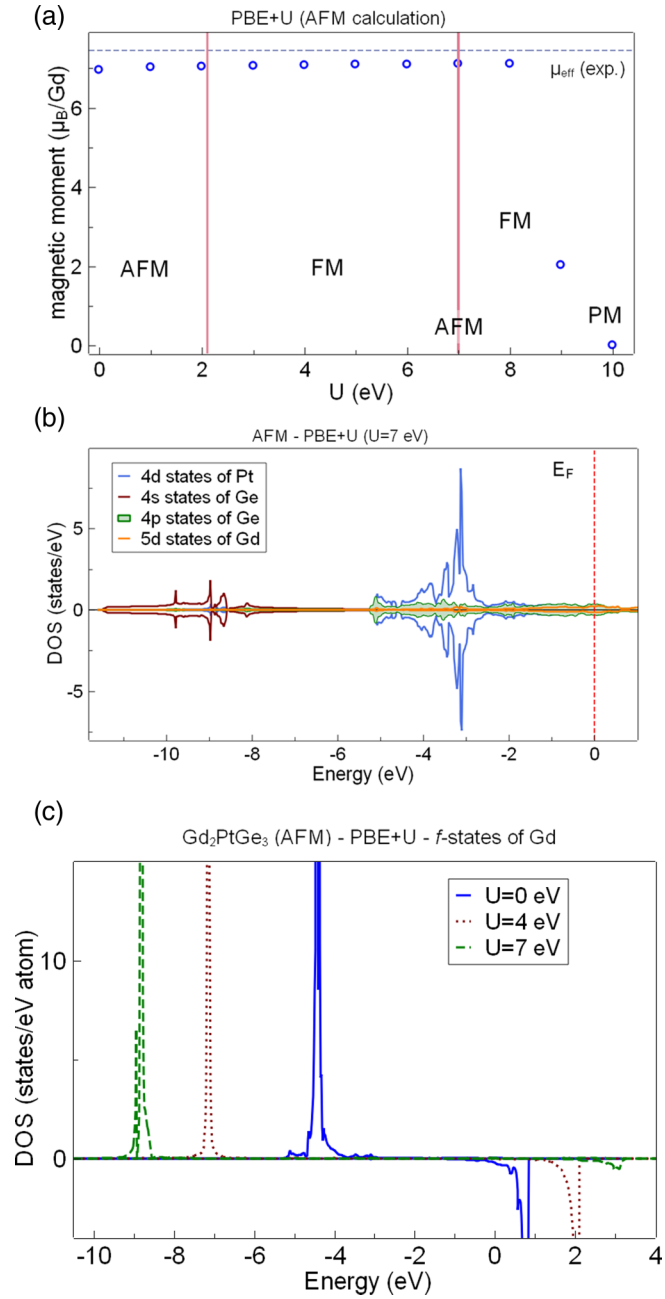

FIG. 7. (a) Gd magnetic moment in Gd_2PtGe_3 as a function of Hubbard U parameter obtained within PBE + U calculations. To facilitate comparison with experimental result the value μ_{eff} is shown as a dashed line. (b) Orbital resolved density of states (DOS) of Pt and Ge atoms in Gd_2PtGe_3. (c) f-projected DOS of Gd based on PBE + U calculations.

the region between -5.5 and -2.2 eV, $4d$ electronic states of Pt make the predominant contribution to the DOS. The Gd $5d$ electronic states contribute to the conduction band. Thus, the d-like bands overlap with the Ge p states of both majority and minority spins. In summary, the combination of GGA in DFT with onsite Coulomb correction U for the $4f$ states of Gd allows us to reliably describe the AFM order in Gd_2PtGe_3. The optimal U value, which is related with increase in intrashell correlation effect in $4f$ states of Gd, turned out to be 7 eV.

The magnetic moment on each Gd was found to be 7.12 μ_B, which is in rather good agreement with the experimental value of μ_{eff} (7.45 μ_B).

IV. CONCLUSIONS

We have successfully synthesized an intermetallic ternary compound Gd_2PtGe_3 by an arc melting technique. The compound forms in a single phase only when the composition is tuned out of the ideal 1:3 stoichiometry ($Gd_2Pt_{1.1}Ge_{2.9}$). The performed magnetic property measurements revealed the existence of long-range AFM ordering in Gd_2PtGe_3 which is very similar to that observed for other members of the Gd_2TGe_3 family. The DC susceptibility measurements allowed us to estimate the negative value of the Curie-Weiss temperature ($\theta_{\text{CW}} = -13$ K), $\mu_{\text{eff}} = 7.45\,\mu_B$, and the transition temperature $T_t = 8$ K. These parameters were used to calculate the empirical measure of the frustration $f = 1.6$, suggesting the presence of intermediately strong magnetic frustration in Gd_2PtGe_3. However, the absence of a shift toward higher temperature with increasing driving frequencies in the plot of the real part of $M_{\text{AC}}(T)$ (Fig. S5 of the Supplemental Material [19]) is inconsistent with a spin-glass-like transition in this compound and suggests a disorder-affected AFM order. The density functional calculations revealed that the Ge 4p and Gd 5d states are the main contributions to the DOS at the Fermi level. The difference between the behavior of Gd_2TGe_3 and other members of the RE_2TGe_3 family underlines the importance of the orbital contribution to the total angular momentum for the formation of glassy magnetic order. Further studies, including local probe methods and neutron spectroscopy, are needed to establish the character of magnetic order in Gd_2TGe_3.

ACKNOWLEDGMENTS

This paper was supported by the Ministry of Science and Higher Education (Poland) under Project No. DIA/2017/014247 ("Diamentowy Grant").

[1] S. Pakhira, C. Mazumdar, R. Ranganathan, S. Giri, and M. Avdeev, Large magnetic cooling power involving frustrated antiferromagnetic spin-glass state in R_2NiSi_3 (R = Gd, Er), Phys. Rev. B **94**, 104414 (2016).

[2] P. Zhi-Yan, C. Chong-De, B. Xiao-Jun, S. Rui-Bo, Z. Jian-Bang, and D. Li-Bing, Structures and physical properties of R_2TX_3 compounds, Chinese Phys. B **22**, 056102 (2013).

[3] R.-D. Hoffmann and R. Pöttgen, AlB_2-related intermetallic compounds—a comprehensive view based on group-subgroup relations, Z. Kristallogr. Cryst. Mater. **216**, 127 (2001).

[4] J. Nagamatsu, N. Nakagawa, T. Muranaka, Y. Zenitani, and J. Akimitsu, Superconductivity at 39 K in magnesium diboride, Nature (London) **410**, 63 (2001).

[5] M. Szlawska, M. Majewicz, and D. Kaczorowski, Ferromagnetic spin-glass behaviour in single-crystalline U_2IrSi_3, J. Phys. Condens. Matter **26**, 126002 (2014).

[6] T. Klimczuk, W. Xie, M. J. Winiarski, R. Koziol, L. Litzbarski, H. Luo an, and R. J. Cava, Crystal structure and physical properties of new Ca_2TGe_3 (T = Pd and Pt) germanides, J. Solid State Chem. **243**, 95 (2016).

[7] A. P. Ramirez, Strongly geometrically frustrated magnets, Annu. Rev. Mater. Sci. **24**, 453 (1994).

[8] M. Frontzek, A. Kreyssig, M. Doerr, A. Schneidewind, J. Hoffmann, and M. Loewenhaupt, Magnetic properties of Tb_2PdSi_3, Phys. B Condens. Matter **350**, E187 (2004).

[9] L. S. Litzbarski, M. J. Winiarski, P. Skokowski, T. Klimczuk, and B. Andrzejewski, Investigation of magnetic order in a new intermetallic compound Nd_2PtGe_3, J. Magn. Magn. Mater. **521**, 167494 (2021).

[10] J. W. Chen, S. Y. Guan, and C. H. Wang, Electrical and magnetic properties of the Ni based ternary compounds R_2NiGe_3 (R = rare earth ions), J. Phys. Conf. Ser. **266**, 012006 (2011).

[11] H. Kito, Y. Takano, and K. Togano, Superconductivity in ternary germanide $Y(Pt_{0.5}Ge_{1.5})$ with the AlB_2-type structure, Phys. C Supercond. **377**, 185 (2002).

[12] S. Majumdar and E. V. Sampathkumaran, Observation of enhanced magnetic transition temperature in Nd_2PdGe_3 and superconductivity in Y_2PdGe_3, Phys. Rev. B **63**, 172407 (2001).

[13] S. Pakhira, C. Mazumdar, and R. Ranganathan, Low-field induced large magnetocaloric effect in $Tm_2Ni_{0.93}Si_{2.93}$: influence of short-range magnetic correlation, J. Phys. Condens. Matter **29**, 505801 (2017).

[14] L. Litzbarski, T. Klimczuk, and M. Winiarski, Synthesis, structure and physical properties of new intermetallic spin glass-like compounds RE_2PdGe_3 (RE = Tb and Dy), J. Phys. Condens. Matter **32**, 225706 (2020).

[15] L. S. Litzbarski, T. Klimczuk, and M. J. Winiarski, $Ho_2Pd_{1.3}Ge_{2.7}$—a ternary AlB_2-type cluster glass system, RSC Adv. **11**, 25187 (2021).

[16] S. Majumdar and E. V. Sampathkumaran, Magnetic behavior of Gd_2CuGe_3: electrical resistance minimum above the Néel temperature, Phys. Rev. B **61**, 43 (2000).

[17] S. Majumdar, M. M. Kumar, and E. V. Sampathkumaran, Magnetic behavior of a new compound, Gd_2PdGe_3, J. Alloys Compd. **288**, 61 (1999).

[18] K. Momma and F. Izumi, VESTA 3 for three-dimensional visualization of crystal, volumetric and morphology data, J. Appl. Cryst. **44**, 1272 (2011).

[19] See Supplemental Material at http://link.aps.org/supplemental/10.1103/PhysRevB.105.054427 for synthesis details, XPS measurements results, and AC magnetization data.

[20] P. E. Blöchl, Projector augmented-wave method, Phys. Rev. B **50**, 17953 (1994).

[21] G. Kresse and D. Joubert, From ultrasoft pseudopotentials to the projector augmented-wave method, Phys. Rev. B **59**, 1758 (1999).

[22] G. Kresse and J. Furthmüller, Efficient iterative schemes for *ab initio* total-energy calculations using a plane-wave basis set, Phys. Rev. B **54**, 11169 (1996).

[23] G. Kresse and J. Furthmüller, Efficiency of *ab-initio* total energy calculations for metals and semiconductors using a plane-wave basis set, Comput. Mater. Sci. **6**, 15 (1996).

[24] J. P. Perdew, K. Burke, and M. Ernzerhof, Generalized Gradient Approximation Made Simple, Phys. Rev. Lett. **77**, 3865 (1996).

[25] R. F. Sabiryanov and S. S. Jaswal, Bulk and surface $4f$ states of Gd, Phys. Rev. B **55**, 4117 (1997).

[26] P. Kurz, G. Bihlmayer, and S. Blügel, Magnetism and electronic structure of hcp Gd and the Gd(0001) surface, J. Phys. Condens. Matter **14**, 6353 (2002).

[27] V. I. Anisimov, F. Aryasetiawan, and A. I. Lichtenstein, First-principles calculations of the electronic structure and spectra of strongly correlated systems: the LDA + U method, J. Phys. Condens. Matter **9**, 767 (1997).

[28] S. Abdelouahed, N. Baadji, and M. Alouani, Electronic structure and x-ray magnetic circular dichroism of gadolinium beyond the local spin density approximation, Phys. Rev. B **75**, 094428 (2007).

[29] C. Schüßler-Langeheine, E. Weschke, C. Mazumdar, R. Meier, A. Y. Grigoriev, G. Kaindl, C. Sutter, D. Abernathy, G. Grubel, and M. Richter, Magnetic splitting of valence states in ferromagnetic and antiferromagnetic lanthanide metals, Phys. Rev. Lett. **84**, 5624 (2000).

[30] S. L. Dudarev, G. A. Botton, S. Y. Savrasov, C. J. Humphreys, and A. P. Sutton, Electron-energy-loss spectra and the structural stability of nickel oxide: an LSDA + U study, Phys. Rev. B **57**, 1505 (1998).

[31] B. N. Harmon, V. P. Antropov, A. I. Liechtenstein, I. V. Solovyev, and V. I. Anisimov, Calculation of magneto-optical properties for $4f$ systems: LSDA + Hubbard U results, J. Phys. Chem. Solids **56**, 1521 (1995).

[32] S. Schulz, A. Yu. Vyazovskaya, G. Poelchen, A. Generalov, M. Güttler, M. Mende, S. Danzenbächer, M. M. Otrokov, T. Balasubramanian, C. Polley, E. V. Chulkov, C. Laubschat, M. Peters, K. Kliemt, C. Krellner, D. Yu. Usachov, and D. V. Vyalikh, Classical and cubic Rashba effect in the presence of in-plane $4f$ magnetism at the iridium silicide surface of the antiferromagnet $GdIr_2Si_2$, Phys. Rev. B **103**, 035123 (2021).

[33] P. Novák, J. Kuneš, L. Chaput, and W. E. Pickett, Exact exchange for correlated electrons, Phys. Status Solidi Basic Res. **243**, 563 (2006).

[34] A. Shick, W. Pickett, and C. Fadley, Electron correlation effects and magnetic ordering at the Gd(0001) surface, Phys. Rev. B **61**, R9213 (2000).

[35] J. Rodríquez-Carvajal and T. Roisnel, Line broadening analysis using FULLPROF*: determination of microstructural properties, Mater. Sci. Forum **443-444**, 123 (2004).

[36] J. A. Mydosh, *Spin Glasses: An Experimental Introduction* (Taylor and Francis, London, 1993).

[37] J. Jensen and A. Mackintosh, *Rare Earth Magnetism: Structures and Excitations* (Clarendon Press, Oxford, 1991).

[38] D. Kaczorowski and H. Noel, Spin-glass-like behaviour in U_2TSi_3 (T identical to Fe, Co, Ni or Cu) intermetallics with disordered AlB_2- and alpha-$ThSi_2$-type structures, J. Phys. Condens. Matter **5**, 9185 (1993).

[39] S. Pakhira, C. Mazumdar, R. Ranganathan, and S. Giri, Chemical disorder driven reentrant spin cluster glass state formation and associated magnetocaloric properties of $Nd_2Ni_{0.94}Si_{2.94}$, Phys. Chem. Chem. Phys. **20**, 7082 (2018).

[40] S. Majumdar, E. V. Sampathkumaran, D. Eckert, A. Handstein, K.-H. Müller, S. R. Saha, H. Sugawara, and H. Sato, Magnetic relaxation behaviour in $Gd_{2-x}Y_xPdSi_3$ alloys, J. Phys.: Condens. Matter **11**, L329 (1999).

[41] J. A. Blanco, D. Gignoux, and D. Schmitt, Specific heat in some gadolinium compounds. II. Theoretical model, Phys. Rev. B **43**, 13145 (1991).

[42] W. M. Farmer, S. F. Skinner, and L. W. Ter Haar, Heat capacity of the highly frustrated triangulated Kagome lattice $Cu_9Cl_2(cpa)_6$, AIP Adv. **8**, 101404 (2018).

[43] B. Koteswararao, R. Kumar, Panchanana Khuntia, S. Bhowal, S. K. Panda, M. R. Rahman, A. V. Mahajan, I. Dasgupta, M. Baenitz, and K. H. Kim, Magnetic properties and heat capacity of the three-dimensional frustrated $S = \frac{1}{2}$ antiferromagnet $PbCuTe_2O_6$, Phys. Rev. B **90**, 035141 (2014).

[44] O. V. Yakubovich, L. V. Shvanskaya, N. B. Bolotina, A. G. Ivanova, G. V. Kiriukhina, I. N. Dovgaliuk, A. S. Volkov, O. V. Dimitrova, and A. N. Vasiliev, An orthorhombic modification of $KCoPO_4$ stabilized under hydrothermal conditions: crystal chemistry and magnetic behavior, Inorg. Chem. **60**, 9461 (2021).

[45] V. Fritsch, J. D. Thompson, and J. L. Sarrao, Spin and orbital frustration in $InCu_4Gd$, Dy, Ho, and Er), Phys. Rev. B **71**, 132401 (2005).

[46] S. Gabani, K. Flachbart, K. Siemensmeyer, and T. Mori, Magnetism and superconductivity of rare earth borides, J. Alloys Compd. **821**, 153201 (2020).

[47] D. A. Joshi, C. V. Tomy, D. S. Rana, R. Nagarajan, and S. K. Malik, Magnetic properties of ternary gallides of type RNi_4Ga (R = rare earths), Solid State Commun. **137**, 225 (2006).

[48] M. Petersen, J. Hafner, and M. Marsman, Structural, electronic and magnetic properties of Gd investigated by DFT + U methods: bulk, clean and H-covered (0001) surfaces, J. Phys. Condens. Matter **18**, 7021 (2006).